THE JOURNAL OF PHYSICAL CHEMISTRY LETTERS
A JOURNAL OF THE AMERICAN CHEMICAL SOCIETY

pubs.acs.org/JPCL

Letter

Limitations of Electrochemical Nitrogen Oxidation toward Nitrate

Hao Wan,* Alexander Bagger, and Jan Rossmeisl

Cite This: J. Phys. Chem. Lett. 2022, 13, 8928–8934

Read Online

ACCESS | Metrics & More | Article Recommendations | Supporting Information

ABSTRACT: The electrocatalytic N_2 oxidation reaction (NOR) using renewable electricity is a promising alternative to the industrial synthesis of nitrate from NH_3 oxidation. However, breaking the triple bond in the nitrogen molecule is one of the most essential challenges in chemistry. In this work, we use density functional theory simulations to investigate the plausible reaction mechanisms of electrocatalytic NOR and its competition with oxygen evolution reaction (OER) at the atomic scale. We focus on the electrochemical conversion of inert N_2 to active *NO during NOR. We propose formation of $*N_2O$ from $*N_2$ and *O as the rate-determining step (RDS). Following the RDS, a microkinetic model is utilized to study the rate of NOR on metal oxides. Our results demonstrate that a lower activation energy is obtained when a catalyst binds *O weakly. We show that the reaction is extremely challenging but also that design strategies have been suggested to promote electrochemical NOR.

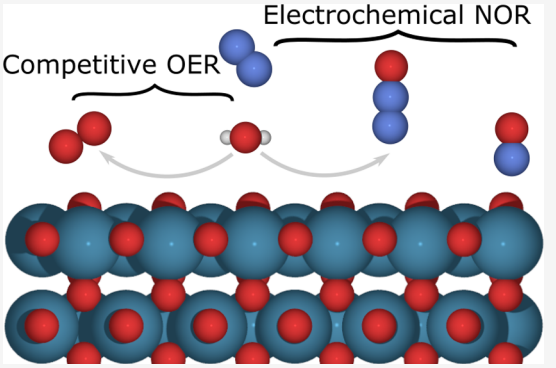

Nitrates are widely used as fertilizers in agriculture and oxidizing agents in explosives.[1,2] Nitrate/nitric acid is manufactured by oxidizing ammonia using the Ostwald process, and the ammonia used here primarily comes from the Haber–Bosch process.[3] These steps involve processes requiring high temperature (~700 K) and high pressure (~150 atm), leading to high energy consumption and large amounts of carbon dioxide emission from the steam reforming process.[4−6] As a result, it is of great interest to bypass the ammonia route and develop a direct and sustainable strategy for nitrate synthesis.[2,7,8]

As a possible approach to produce nitrogen oxides and ultimately nitrate,[1,5] direct nitrogen oxidation is, however, extremely slow at ambient conditions, and only very high temperatures or plasmas enable reasonable reaction rates.[9−11] Electrochemical oxidative fixation of nitrogen appears to be a very attractive approach which could be driven by the electricity at ambient conditions, making the process sustainable. Figure 1a shows thermodynamic potentials at a reversible hydrogen electrode (RHE) potential scale for some important reactions, such as water oxidation and nitrogen reduction and oxidation. Even though direct N_2 oxidation with O_2 provides a possible solution from the thermodynamic point of view, the conflicts between O_2 dissociation, where strong *O adsorption catalysts are needed,[12] and N_2 activation, which demands a weak *O adsorption catalyst,[13] limit the O_2 as the reactant. It can be seen that the reaction $(N_2(g) + 6H_2O(l) \rightarrow 2HNO_3(g) + 10(H^+ + e^-))$ has an equilibrium potential of 1.32 V vs RHE, and it has been suggested that nitrate ion production is thermodynamically favored over the competitive oxygen evolution reaction (OER) at pH above 1.3 in a wide potential region.[5] In the past two years, a few materials, such as Pd/MXenes,[14] several oxides (spinel oxide,[15] Ru/TiO_2,[16] and PdO_2-based[17,18]) were reported as potential electrocatalysts for NOR toward nitrate.[19−23] Figure 1b,c displays Faradaic efficiency (FE) and yields for nitrate formation from experiments. As can be observed, the FE and currents are low because of the severely competitive OER.

For electrochemical NOR, it has been proposed that the nitrate formation from N_2 oxidation can be divided into two steps: (i) the conversion of N_2 into the *NO intermediate (* denotes the active site) and (ii) the transformation of *NO to nitrate. The former is an electrocatalytic process, which is considered as the rate-limiting step;[13] the latter is a non-electrochemical redox reaction where the conversion of NO to HNO_3 is known to occur readily through reaction with water.[24] As a result, uncovering the conversion N_2 toward *NO is needed in order to understand the electrochemical NOR.

In this study, the goal is to contribute to the understanding of the electrochemical NOR by establishing a theoretical framework. We aim to provide design strategies for NOR electrocatalysts both in terms of reaction rates and selectivity toward N_2 oxidation relative to oxygen evolution reaction, OER. For the activation of N_2, we evaluate different pathways

Received: August 8, 2022
Accepted: September 19, 2022
Published: September 21, 2022

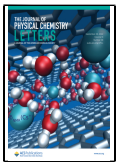

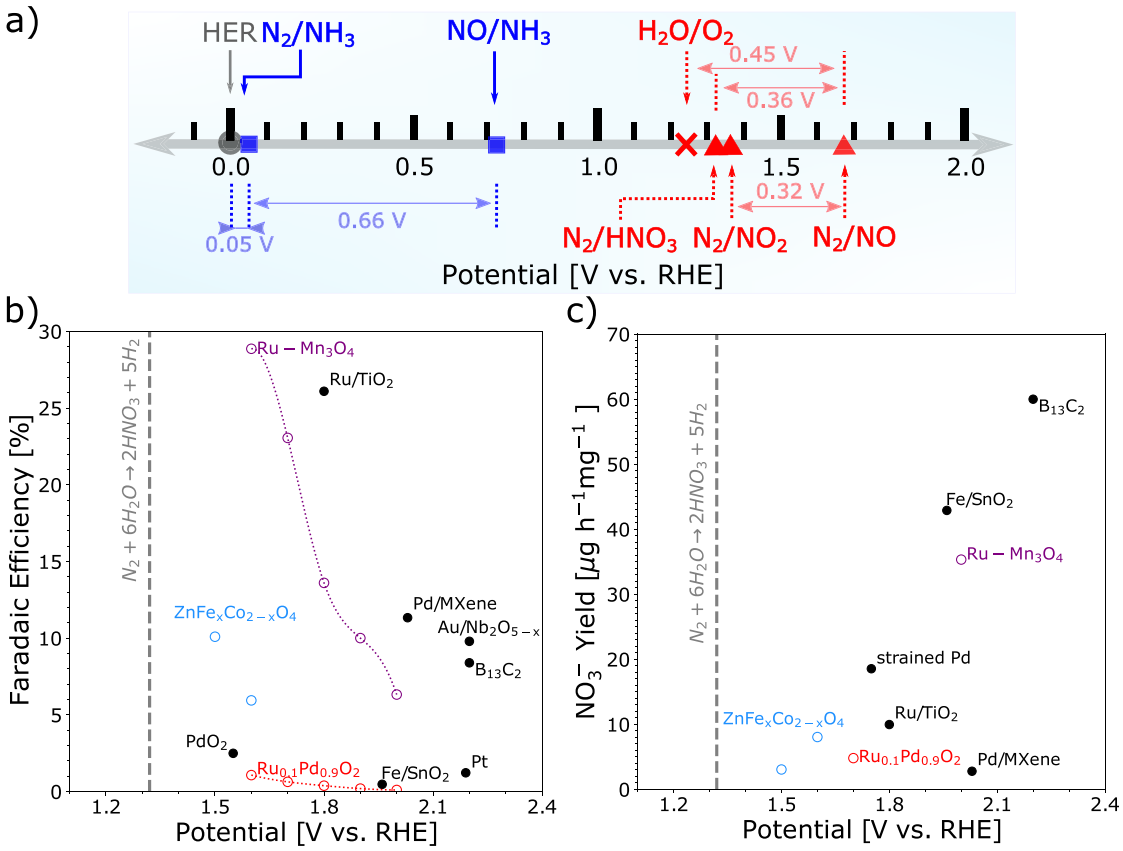

Figure 1. (a) Redox couples for nitrogen reduction (blue) and oxidation (red) with thermodynamic potentials. Note HNO_3 is gas. The difference between oxygen evolution and nitrogen oxidation is shown to highlight the selectivity challenge for nitrogen oxidation. (b) Experimental reported faradaic efficiency and (c) yield of nitrate production for NOR on different materials, like Pd/MXenes,[14] spinel oxide,[15] Ru/TiO_2,[16] PdO_2-based,[17,18] Pt,[19] Fe/SnO_2,[20] Au/Nb_2O_{5-x},[21] $B_{13}C_{12}$,[22] and Ru–Mn_3O4[23] against potentials. The gray vertical line indicates the equilibrium potential of NOR toward HNO_3.

and investigate the activation barriers to identify a possible rate-determining step in NOR. A classification scheme is utilized to investigate key intermediates (e.g., $*N_2O$ and *NO) during the activation of N_2 among a class of metal oxide catalysts. The adsorption energy of $*N_2$ and the adsorption energy difference between *O and *OH have been applied to describe the competition between OER and NOR. On this basis, we suggest the limitations of electrochemical NOR toward nitrate.

For electrochemical N_2 activation, we consider the N_2 triple bond to be activated via three different pathways as seen in Figure 2. (I) Dissociative path: direct dissociation of N_2 is possible, when the metal oxides have a strong nitrogen adsorption.[25] (II) Hydroxy path: the N_2 is activated by a water molecule, forming $*N_2OH$. (III) Oxygen path: N_2 activation is achieved via reaction with an adsorbed *O.

Figure 3 show simulations for the N_2 activations via the three different paths: (I) dissociative path, (II) hydroxy path, and (III) oxygen path. Following (I) the dissociative path, a Brønsted–Evans–Polanyi (BEP) relation for $N_2(g) + 2* \rightarrow 2*N$, is obtained with a slope close to 1 as shown in Figure 3a. Metal oxides with a weaker 2*N binding demand a higher activation energy. Most metal oxides investigated here require energy above 1 eV, indicating that the direct N_2 dissociation is unlikely. With respect to (II) the hydroxy path, Figure 3b shows that the direct hydoxy to $*N_2$ from H_2O for $*N_2OH$ formation is unfavorable with a thermodynamic binding above 1.6 eV, compared to *OH adsorption on metal oxides. As a comparison, N_2 activation via adsorbed *OH: $N_2 + *OH \rightarrow *N_2OH$ is also considered (see Figure S1), and it has been observed that the required energy is beyond 2 eV for all metal oxides. As for (III) the oxygen path, Figure 3c shows that the activation barrier for $*N_2O$ formation from $*N_2 + *O$ scales with the *O adsorption energy with a slope close to −1. A lower energy barrier is found on metal oxides with a weaker *O adsorption energy. For example, metal oxides like SnO_2, TiO_2, and PdO_2 are interesting candidates with activation energies below 1 eV. As a result, for electrochemical NOR, N_2 might be activated via the oxygen path: $N_2(g) + *O \rightarrow *N_2O$ on weak oxygen binding oxides. Additionally, N_2 activation via surface lattice oxygen (Mars Van Krevelen mechanism, Figure S2) also has been investigated where a lower driving force (more positive Gibbs free energy change) and a higher activation barrier are observed. Further NO formation from $*N_2O + *O$ shows a lower activation barrier (see Figure S3). Hence, the activation of N_2 with the adsorbed *O is the rate-limiting step.

As a competition for NOR, the parasitic OER has to be considered. A classification approach is utilized for understanding the competition between OER and NOR, which is similar to previous work related to $CO_2/NO/N_2$ reductions.[26−29] First, the molecular adsorption of N_2, N_2O, and NO is simulated. Figure 4a shows that the $*N_2$ adsorption energy is plotted against the adsorption energy of $*N_2O$ (ΔE_{*N_2O}) on

https://doi.org/10.1021/acs.jpclett.2c02459
J. Phys. Chem. Lett. 2022, 13, 8928−8934

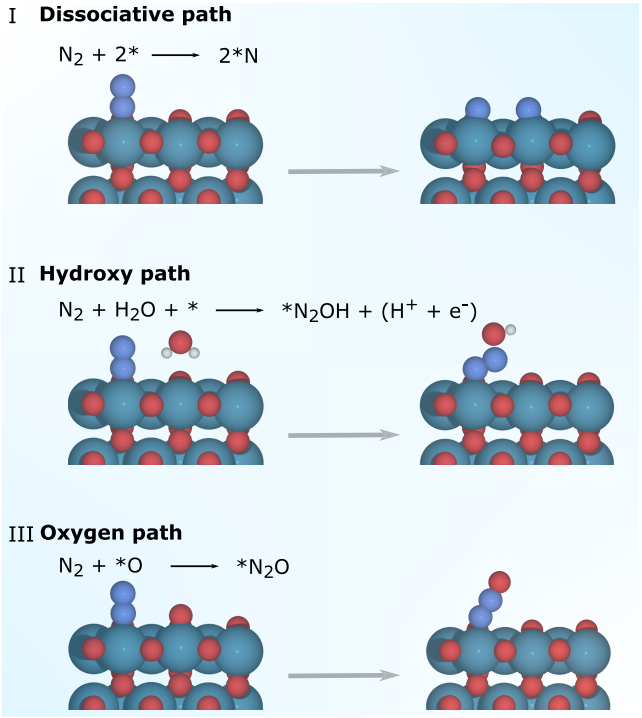

Figure 2. Scheme for N_2 activation: (I) Dissociative path: $N_2(g) + 2^* \rightarrow 2^*N$; (II) Hydroxy path: $N_2(g) + H_2O \rightarrow {}^*N_2OH + (H^+ + e^-)$; (III) Oxygen path: $N_2(g) + {}^*O \rightarrow {}^*N_2O$.

metal oxide catalysts where a close correlation between these two intermediates is observed. The horizontal dotted line demonstrates the equilibrium between $N_2(g) + * \rightarrow {}^*N_2$, while the vertical line illustrates the equilibrium between $N_2O(g) + * \rightarrow {}^*N_2O$. Three groups of catalysts can be identified: (1) both $^*N_2$ and $^*N_2O$ adsorption are favorable, such as IrO_2; (2) both $^*N_2$ and $^*N_2O$ adsorption are unfavorable, like SnO_2, TiO_2, and PtO_2; (3) binding $^*N_2O$ but not $^*N_2$, like RuO_2. This suggests that metal oxides in group 1, such as IrO_2, might be capable of activating the N_2 molecule because of its strong interaction, and it can be noted that the metal oxides which can bind the N_2 can also bind N_2O. Figure 4b shows the adsorption energies of $^*N_2$ vs *NO on metal oxide catalysts. All catalysts except SnO_2 and TiO_2 bind *NO. Further, the competition of OER is then considered using a microkinetic model.

One of the possible microkinetic models that can be considered for N_2 oxidation assumes that N_2O formation is the rate-determining step, which is suggested from Figures 3 and S3. To keep the kinetic model simple but still capturing the important chemistry, we consider the following reactions:

$$N_2 + * \xrightarrow{K_1} {}^*N_2 \quad (1)$$

$$H_2O + * \xrightarrow{K_2} {}^*O + 2H^+ + 2e^- \quad (2)$$

$${}^*N_2 + {}^*O \underset{k_3^-}{\overset{k_3^+}{\rightleftarrows}} {}^*N_2O \quad \text{(RDS)} \quad (3)$$

$${}^*N_2O + {}^*O \xrightarrow{K_4} 2{}^*NO \quad (4)$$

$${}^*NO \xrightarrow{K_5} * + NO \quad (5)$$

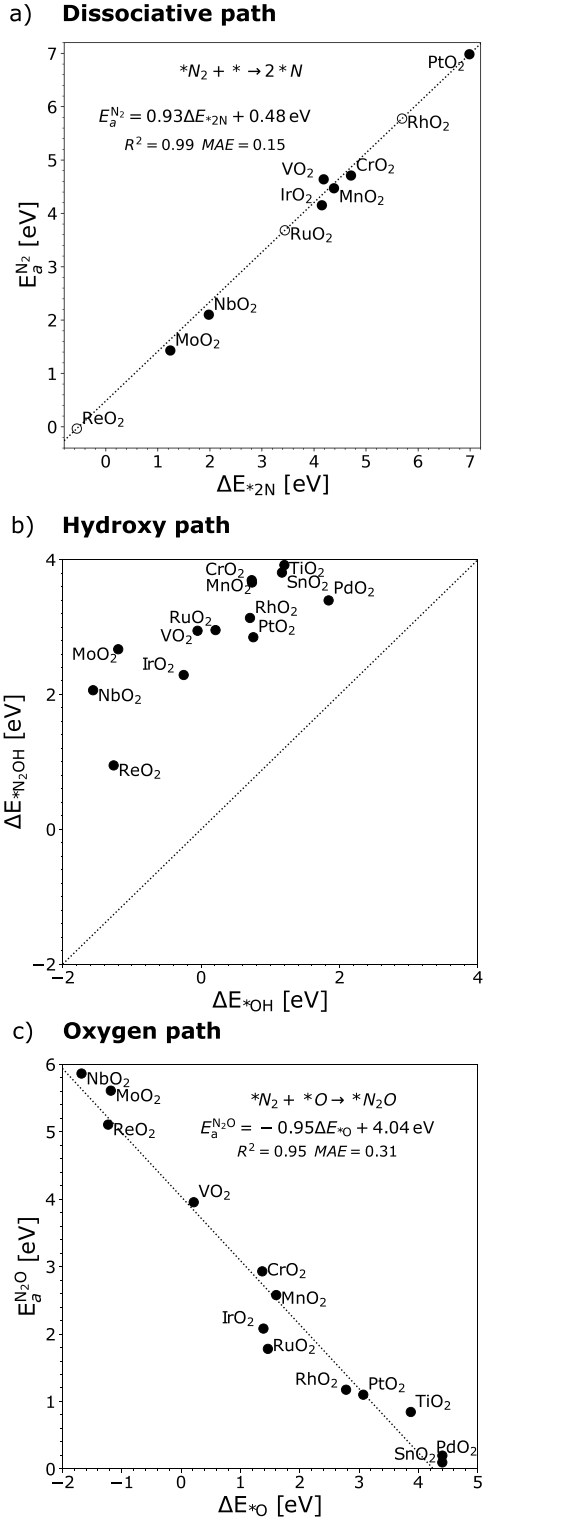

Figure 3. (a) Calculated transition state energy $\Delta E_a^{N_2}$ for N_2 dissociation as a function of dissociative chemisorption energy ΔE_{*2N}. Here, unfilled markers are obtained from the linear fitting. (b) The adsorption energy of $^*N_2OH$ plotted against the *OH adsorption energy. The diagonal line shows the equal adsorption for *OH and $^*N_2OH$. (c) Calculated transition state energy $\Delta E_a^{N_2O}$ for $^*N_2 + {}^*O \rightarrow {}^*N_2O$ against *O adsorption energy. Considering the scaling between ΔE and ΔE_{*O} (Figure S4), and then $\Delta E_a^{N_2O} \approx \Delta E + 1.24$ eV. It should be noted that N_2 adsorption is unfavorable for most metal oxides.

https://doi.org/10.1021/acs.jpclett.2c02459
J. Phys. Chem. Lett. 2022, 13, 8928−8934

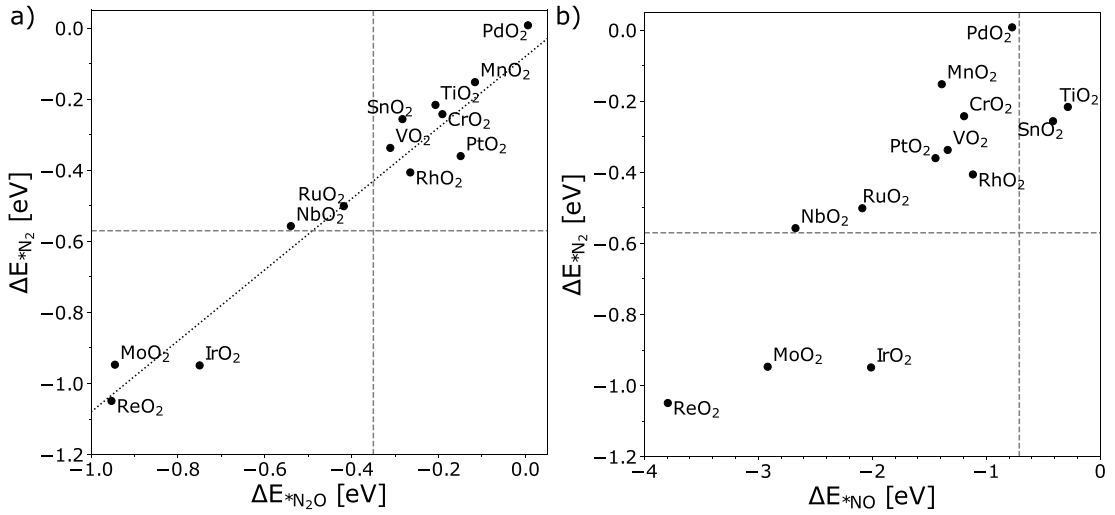

Figure 4. Adsorption energies of the intermediates (a) $*N_2$ vs $*N_2O$ and (b) $*N_2$ vs *NO. The horizontal lines demonstrate the equilibrium between $N_2(g) + * \rightarrow *N_2$, while the vertical line in panel a illustrates the equilibrium between $N_2O(g) + * \rightarrow *N_2O$ and the vertical line in panel b represents the equilibrium between $NO(g) + * \rightarrow *NO$.

$$H_2O + *O \xrightarrow{k_6^+} * + O_2 + 2H^+ + 2e^- \quad (6)$$

For each step in quasi-equilibrium we can use the Langmuir isotherm:

$$\theta_{N_2} = K_1 P_{N_2} \theta_* \quad (7)$$

$$\theta_O = K_2 P_{H_2O} \theta_* \quad (8)$$

$$\theta_{NO} = K_5^{-1} P_{NO} \theta_* \quad (9)$$

$$\theta_{N_2O} = K_2^{-1} K_4^{-1} K_5^{-2} P_{NO}^2 P_{H_2O}^{-1} \theta_* \quad (10)$$

$$\theta_{N_2} + \theta_O + \theta_{NO} + \theta_{N_2O} + \theta_* = 1 \quad (11)$$

At low temperatures, the surface will be dominated by adsorbed *O, such that *O is the most abundant reaction intermediate, implying that θ_* can be written as

$$\theta_* = \frac{1}{1 + K_2 P_{H_2O}} \quad (12)$$

Assuming that eqs 1, 2, and 4 are quasi-equilibrated for NOR and that the total number of catalytic sites is fixed leads to the following analytical expression for the rate of nitrogen oxidation (R(NOR); for more details, see the Supporting Information). As for the rate of water oxidation (R(OER)) for promising NOR catalysts which can provide a reactive *O, like PtO_2, TiO_2, SnO_2, and PdO_2 (see Figure 5a), it is limited by the formation of *O (eq 2) which is potential-dependent.

$$R(NOR) = k_3^+ K_1 K_2 P_{N_2} P_{H_2O} \left(1 - \frac{P_{NO}^2}{K_{TOT} P_{N_2} P_{H_2O}^2}\right) \theta_*^2 \quad (13)$$

$$R(OER) = k_2^+ P_{H_2O} \theta_* \quad (14)$$

The Faradiac efficiency (FE) for NOR is then defined by

$$FE = \frac{R(NOR)}{R(NOR) + R(OER)} \times 100\% \quad (15)$$

The reaction constant k_3^+ for eq 3 can be calculated from transition-state theory (TST) while the equilibrium constants for eq 1 (K_1), eq 2 (K_2), and the overall reaction (K_{TOT}) can be computed as shown in eqs 16, 17, and 18.

$$K_1 = \exp(-\Delta G_{rxn,1}/k_B T)$$
$$K_2 = \frac{k_2^+}{k_2^-} = \exp(-\Delta G_{rxn,2}/k_B T) \quad (16)$$

$$k_2^+ = \frac{k_B T}{h} \exp(-\Delta G_{rxn,2}/k_B T)$$
$$k_3^+ = \frac{k_B T}{h} \exp(-\Delta G_{TS,3}/k_B T) \quad (17)$$

$$K_{TOT} = \exp(-\Delta G_{TOT}/k_B T) \quad (18)$$

where $\Delta G_{rxn,1}$ and $\Delta G_{rxn,2}$ are the reaction energy for eqs 1 and 2, respectively. Following the Gibbs free energy change $\Delta G_{rxn,2}$ for the reaction in eq 16, the rate constant k_2^+ can be expressed as $k_2^+ = \frac{k_B T}{h} \exp[(-\Delta G_{*O} - 2eU_{RHE})/k_B T]$ where U_{RHE} is the applied potential, indicating that k_2^+ is potential-dependent. The rate constant, k_3^+, in eq 17 does not depend on the applied potential as this is a purely thermal heterogeneous catalytic step. The above expression for FE (eq 15) is written explicitly in terms of the pressure of the reactant (N_2) and product (NO) relative to the standard state pressure (1 bar). In the following analysis, the influence from O_2 partial pressure is not included, since there is a limited impact from the change of the O_2 chemical potential under a high O_2 partial pressure. Here, FE can be approximated using only two independent electronic energy parameters: N_2 adsorption energy (ΔE_{*N_2}) and O adsorption energy (ΔE_{*O}).

In Figure 5a, the OER activity volcano is plotted as a function of $\Delta E_{*O} - \Delta E_{*OH}$. In Figure 5b, a 2-D activity heatmap also employs $\Delta E_{*O} - \Delta E_{*OH}$ as a parameter, with the utilization of scaling relation between ΔE_{*O} and $\Delta E_{*O} - \Delta E_{*OH}$ (see Figure S6). As a result, a 2-D activity heatmap for FE of NOR can be constructed based on these two descriptors as shown in Figure 5b where FE is computed at a temperature of 300 K with applied potential of $U_{RHE} = (\Delta G_{*O} - \Delta G_{*OH})/e$ to fix *O coverage. This applied potential is also intended for

https://doi.org/10.1021/acs.jpclett.2c02459
J. Phys. Chem. Lett. 2022, 13, 8928−8934

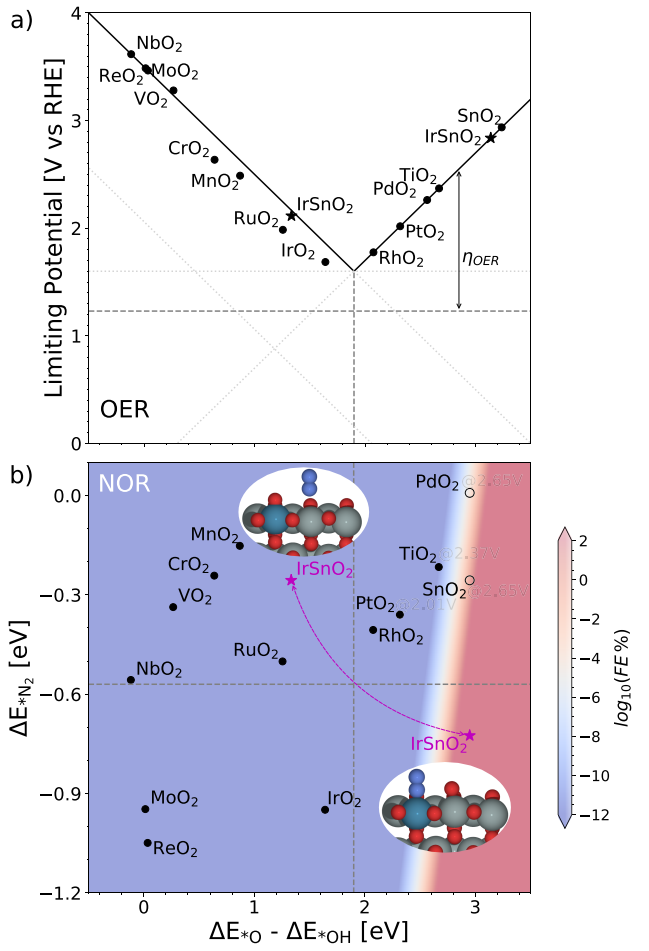

Figure 5. (a) OER activity volcano: the limiting potential vs $\Delta E_{*O} - \Delta E_{*OH}$. The horizontal dashed line is the theoretical value (1.23 V) for OER. (b) 2-D activity heatmap describing FE (here, $\log_{10}$FE is employed) for the nitrogen oxidation as a function of $(\Delta E_{*O} - \Delta E_{*OH})$ and ΔE_{*N_2}, computed at a temperature of 300 K with (a) $P_{N_2} = 1$, $P_{H_2O} = 1$. It is important to note that the coverage of *O is kept fixed by applying a potential of $(\Delta E_{*O} - \Delta E_{*OH})/e$. The vertical dotted line demonstrates the optima of $\Delta E_{*O} - \Delta E_{*OH}$ for providing best OER catalytic activity. It should be noted that $\Delta E_{*O} - \Delta E_{*OH}$ of SnO_2, PdO_2 (unfilled markers) have been adjusted using the scaling relation in Figure S6 in order to obtain simulated $\Delta E_a^{N_2O}$. Structures in panel b: $IrSnO_2$. O, red; N, blue; Sn, gray; Ir, royal blue.

adsorbed *O to be thermodynamically stable at the surface. The vertical dotted line demonstrates the optima of $\Delta E_{*O} - \Delta E_{*OH}$ for providing best OER catalytic activity.

Figure 5b shows that the FE toward NO for almost all oxides is extremely low, and only SnO_2 and PdO_2 show limited FE for NOR under conditions of $P_{N_2} = 1$, $P_{H_2O} = 1$ with temperature at 300 K. Further increasing the partial pressure for N_2 or decreasing the content of H_2O (see Figure S7) has only a limited improvement for the activity toward NOR, and still the OER dominates. Clearly, NOR is limited compared to OER. However, the heatmap indicates that a higher activity for NOR can be obtained when a catalyst has a stronger N_2 adsorption and a weaker *O adsorption. As a result, mixing a weak *O adsorption catalyst like TiO_2, PdO_2, or SnO_2 with strong N_2 binding sites like Fe, Ir, and Ru could provide higher NOR activity. For example, experimentally it has been reported that Ru-doped TiO_2 enabled a nitrate yield rate of 10.04 μg $h^{-1}mg^{-1}$ with an FE of 26.1%[16] and Fe-SnO_2 demonstrated a nitrate yield rate of 42.9 μg $h^{-1}mg^{-1}$ with an FE of 0.84%.[20] Here, some bimetallic oxides, including $RuTiO_2$, $IrTiO_2$, $IrPdO_2$, and $IrSnO_2$, which are computationally constructed by the second metal atom replaced with the first metal atom, have been investigated. For example, $IrSnO_2$ is constructed by the substitution of surface Sn with Ir in SnO_2 bulk (see structures in Figure 5b). As suggested in Figure 5b, $IrSnO_2$ might be an interesting candidate for NOR ($\Delta E_a^{N_2O} \approx 0.34$ eV, see Figure S8) when $*N_2$ is adsorbed on Ir while *O sits on Sn (magenta star in red area). However, the competition might also exist if *O is adsorbed on Ir, where there is no NOR activity (the magenta star in the blue area). As for other bimetallic oxides, no NOR catalytic activity is observed because of either a weak N_2 binding ($RuTiO_2$ and $IrPdO_2$) or a relatively strong *O adsorption ($RuTiO_2$, $IrTiO_2$, and $IrPdO_2$; see Table S4).

Another more promising strategy for higher intrinsic catalytic NOR activity and selectivity is to find catalysts with a better BEP for $N_2(g) + *O \rightarrow *N_2O$. The ideal BEP for this $*N_2O$ formation is activation energy $\Delta E_a^{N_2O}$ close to the reaction energy ΔE. This can be achieved by stabilizing the transition state relative to the final state. In other words, the transition state and final state should have a similar adsorption configuration, which has been employed on electrochemical O_2 reduction by using dual-site (diporphyrin) catalysts.[12,30] To be more specific, there is around 1.24 eV intercept difference between the BEP on metal oxides and the ideal BEP relation. On metal oxides (Figure S8), the tilting and returning process of $*N_2$ during $*N_2O$ formation contributes to the extra barrier (1.24 eV) to overcome except the reaction energy difference part. Eliminating the tilting and returning of $*N_2$ will move the BEP toward the ideal situation. This can be achieved by constructing another three-dimensional active site similar to the structure of diporphyrin to have adsorbed *O right above the adsorbed $*N_2$, not like the neighboring adsorption in metal oxides. The other active site serves as an *O shuttle, which does not require the $*N_2$ tilting or moving as shown in Figure S9. With the utilization of the ideal BEP relation, the stronger *O binding area is unlocked for higher NOR activity and selectivity (see Figure S10).

In this study, we use DFT simulations to investigate the possibility of the electrochemical NOR over rutile metal oxide catalysts. During the NOR process, the OER is a parasitic reaction on all metal oxides and a grand challenge to avoid. A fundamental surface catalytic limitation in terms of a compromise between selectivity and activity of NOR is identified. Similar to electrochemical N_2 reduction, one of the challenges is really that N_2 does not bind particularly strongly on any catalyst even though binding N_2 on the oxides is slightly stronger than on metals.[29] Our results propose the activation of N_2 with *O forming $*N_2O$ as the rate-limiting step. Via changing the catalytic surface, it is possible to tune the reactivity of an adsorbed *O atom. This correlates with the activation energy required to activate N_2. A less stable oxygen binding catalyst, i.e., a catalyst providing a more reactive *O, such as PdO_2 and SnO_2, results in a lower energy barrier to overcome for $*N_2O$ formation. Consequently, a higher potential needs to be applied. A 2-D activity heatmap constructed via a simple mircokinetic model demonstrates that in addition to a weaker *O adsorption, a fairly strong N_2 adsorption might also promote a higher NOR activity. These suggest that systems mixing a weaker *O adsorption bulk like

https://doi.org/10.1021/acs.jpclett.2c02459
J. Phys. Chem. Lett. 2022, 13, 8928−8934

PdO_2 and SnO_2 with a strong N_2 binding site, like Fe, Ru, or Ir, can be interesting candidates. These results possibly explain the experimental observation where some electrochemical NOR activity was observed on systems such as Fe-SnO_2 and Ru-PdO_2. Following these results, Ir-SnO_2 has been investigated as another possible candidate for NOR when Sn has *O adsorbed and N_2 binds on Ir. In addition, a higher N_2 pressure and low water content also slightly promote NOR over OER. Finding electrocatalysts with a more favorable BEP for N_2O formation can be another promising strategy for the desired NOR. These findings might benefit the way for the design and discovery of the selective and active NOR electrocatalysts. Future work for a more comprehensive investigation of bimetallic oxides might be interesting to further explore with the aim of higher selectivity. Computationally, beyond-generalized gradient approximation (GGA) approaches such GGA+U or hybrids might be interesting to be utilized to investigate the defect/polaron states in catalysts.[31] In addition, grand canonical DFT[32−34] could be further employed in the future to explore other possible reaction pathways and explicit dependence on pH, applied potential, surface coverages, and ions for a more detailed understanding of NOR.

■ ASSOCIATED CONTENT

Supporting Information

The Supporting Information is available free of charge at https://pubs.acs.org/doi/10.1021/acs.jpclett.2c02459.

Computational details, including different exchange correlation functionals comparison, water impact on adsorption energies, and microkinetic model construction (PDF)

■ AUTHOR INFORMATION

Corresponding Author

Hao Wan − *Fritz Haber Institute of the Max Planck Society, 14195 Berlin, Germany;* orcid.org/0000-0002-7489-3433; Email: wan@fhi-berlin.mpg.de

Authors

Alexander Bagger − *Center for High Entropy Alloy Catalysis (CHEAC), Department of Chemistry, University of Copenhagen, DK-2100 Copenhagen, Denmark;* orcid.org/0000-0002-6394-029X

Jan Rossmeisl − *Center for High Entropy Alloy Catalysis (CHEAC), Department of Chemistry, University of Copenhagen, DK-2100 Copenhagen, Denmark;* orcid.org/0000-0001-7749-6567

Complete contact information is available at: https://pubs.acs.org/10.1021/acs.jpclett.2c02459

Funding

Open access funded by Max Planck Society.

Notes

The authors declare no competing financial interest.

■ ACKNOWLEDGMENTS

We acknowledge support from the Research Grant 9455 from Villum Fonden. The Center for High Entropy Alloys Catalysis is sponsored by the Danish National Research Foundation centers of excellence, Project DNRF149.

■ REFERENCES

(1) Medford, A. J.; Hatzell, M. C. Photon-Driven Nitrogen Fixation: Current Progress, Thermodynamic Considerations, and Future Outlook. *ACS Catal.* **2017**, *7*, 2624−2643.

(2) Lim, J.; Fernández, C. A.; Lee, S. W.; Hatzell, M. C. Ammonia and Nitric Acid Demands for Fertilizer Use in 2050. *ACS Energy Lett.* **2021**, *6*, 3676−3685.

(3) Valera-Medina, A.; Xiao, H.; Owen-Jones, M.; David, W.; Bowen, P. Ammonia for power. *Prog. Energy Combust. Sci.* **2018**, *69*, 63−102.

(4) Schlögl, R. Catalytic Synthesis of Ammonia—A "Never-Ending Story. *Angew. Chem., Int. Ed.* **2003**, *42*, 2004−2008.

(5) Chen, J. G.; Crooks, R. M.; Seefeldt, L. C.; Bren, K. L.; Bullock, R. M.; Darensbourg, M. Y.; Holland, P. L.; Hoffman, B.; Janik, M. J.; Jones, A. K.; Kanatzidis, M. G.; King, P.; Lancaster, K. M.; Lymar, S. V.; Pfromm, P.; Schneider, W. F.; Schrock, R. R. Beyond fossil fuel-driven nitrogen transformations. *Science* **2018**, *360*, No. eaar6611.

(6) Andersen, S. Z.; Čolić, V.; Yang, S.; Schwalbe, J. A.; Nielander, A. C.; Mcenaney, J. M.; Enemark-Rasmussen, K.; Baker, J. G.; Singh, A. R.; Rohr, B. A.; Statt, M. J.; Blair, S. J.; Mezzavilla, S.; Kibsgaard, J.; Vesborg, P. C. K.; Cargnello, M.; Bent, S. F.; Jaramillo, T. F.; Stephens, I. E. L.; Nørskov, J. K.; Chorkendorff, I. A rigorous electrochemical ammonia synthesis protocol with quantitative isotope measurements. *Nature* **2019**, *570*, 504−508.

(7) Baltrusaitis, J. Sustainable Ammonia Production. *ACS Sustainable Chem. Eng.* **2017**, *5*, 9527.

(8) Iriawan, H.; Andersen, S. Z.; Zhang, X.; Comer, B.; Barrio, J.; Chen, P.; Medford, A.; Stephens, I. E. L.; Chorkendorff, I.; Shao-Horn, Y. Nitrogen Activation by Reduction and Oxidation. *Nature Reviews Methods Primers* **2021**, *1*, 56.

(9) Wang, Y.; DeSilva, A. W.; Goldenbaum, G. C.; Dickerson, R. R. Nitric oxide production by simulated lightning: Dependence on current, energy, and pressure. *Journal of Geophysical Research: Atmospheres* **1998**, *103*, 19149−19159.

(10) Cherkasov, N.; Ibhadon, A.; Fitzpatrick, P. A review of the existing and alternative methods for greener nitrogen fixation. *Chemical Engineering and Processing: Process Intensification* **2015**, *90*, 24−33.

(11) Rouwenhorst, K. H. R.; Jardali, F.; Bogaerts, A.; Lefferts, L. From the Birkeland−Eyde process towards energy-efficient plasma-based NOX synthesis: a techno-economic analysis. *Energy Environ. Sci.* **2021**, *14*, 2520−2534.

(12) Wan, H.; Jensen, A. W.; Escudero-Escribano, M.; Rossmeisl, J. Insights in the Oxygen Reduction Reaction: From Metallic Electrocatalysts to Diporphyrins. *ACS Catal.* **2020**, *10*, 5979−5989.

(13) Anand, M.; Abraham, C. S.; Nørskov, J. K. Electrochemical oxidation of molecular nitrogen to nitric acid − towards a molecular level understanding of the challenges. *Chem. Sci.* **2021**, *12*, 6442−6448.

(14) Fang, W.; Du, C.; Kuang, M.; Chen, M.; Huang, W.; Ren, H.; Xu, J.; Feldhoff, A.; Yan, Q. Boosting efficient ambient nitrogen oxidation by a well-dispersed Pd on MXene electrocatalyst. *Chem. Commun.* **2020**, *56*, 5779−5782.

(15) Dai, C.; Sun, Y.; Chen, G.; Fisher, A. C.; Xu, Z. J. Electrochemical Oxidation of Nitrogen towards Direct Nitrate Production on Spinel Oxides. *Angew. Chem., Int. Ed.* **2020**, *59*, 9418−9422.

(16) Kuang, M.; Wang, Y.; Fang, W.; Tan, H.; Chen, M.; Yao, J.; Liu, C.; Xu, J.; Zhou, K.; Yan, Q. Efficient Nitrate Synthesis via Ambient Nitrogen Oxidation with Ru-Doped TiO2/RuO2 Electrocatalysts. *Adv. Mater.* **2020**, *32*, 2002189.

(17) Han, S.; Wang, C.; Wang, Y.; Yu, Y.; Zhang, B. Electrosynthesis of Nitrate via the Oxidation of Nitrogen on Tensile-Strained Palladium Porous Nanosheets. *Angew. Chem., Int. Ed.* **2021**, *60*, 4474−4478.

(18) Li, T.; Han, S.; Wang, C.; Huang, Y.; Wang, Y.; Yu, Y.; Zhang, B. Ru-Doped Pd Nanoparticles for Nitrogen Electrooxidation to Nitrate. *ACS Catal.* **2021**, *11*, 14032−14037.

(19) Wang, Y.; Yu, Y.; Jia, R.; Zhang, C.; Zhang, B. Electrochemical synthesis of nitric acid from air and ammonia through waste utilization. *National Science Review* **2019**, *6*, 730−738.
(20) Zhang, L.; Cong, M.; Ding, X.; Jin, Y.; Xu, F.; Wang, Y.; Chen, L.; Zhang, L. A Janus Fe-SnO2 Catalyst that Enables Bifunctional Electrochemical Nitrogen Fixation. *Angew. Chem., Int. Ed.* **2020**, *59*, 10888−10893.
(21) Zhang, Y.; Du, F.; Wang, R.; Ling, X.; Wang, X.; Shen, Q.; Xiong, Y.; Li, T.; Zhou, Y.; Zou, Z. Electrocatalytic fixation of N2 into NO3-: electron transfer between oxygen vacancies and loaded Au in Nb2O5-x nanobelts to promote ambient nitrogen oxidation. *J. Mater. Chem. A* **2021**, *9*, 17442−17450.
(22) Lan, J.; Luo, M.; Han, J.; Peng, M.; Duan, H.; Tan, Y. Nanoporous B13C2 towards Highly Efficient Electrochemical Nitrogen Fixation. *Small* **2021**, *17*, 2102814.
(23) Nie, Z.; Zhang, L.; Ding, X.; Cong, M.; Xu, F.; Ma, L.; Guo, M.; Li, M.; Zhang, L. Catalytic Kinetics Regulation for Enhanced Electrochemical Nitrogen Oxidation by Ru Nanoclusters-Coupled Mn3O4 Catalysts Decorated with Atomically Dispersed Ru Atoms. *Adv. Mater.* **2022**, *34*, 2108180.
(24) *Ullmann's encyclopedia of industrial chemistry*, 6th ed.; Wiley-VCH: Weinheim, Germany, 2003.
(25) Vojvodic, A.; Calle-Vallejo, F.; Guo, W.; Wang, S.; Toftelund, A.; Studt, F.; Martínez, J. I.; Shen, J.; Man, I. C.; Rossmeisl, J.; Bligaard, T.; Nørskov, J. K.; Abild-Pedersen, F. On the behavior of Brønsted-Evans-Polanyi relations for transition metal oxides. *J. Chem. Phys.* **2011**, *134*, 244509.
(26) Bagger, A.; Ju, W.; Varela, A. S.; Strasser, P.; Rossmeisl, J. Electrochemical CO2 Reduction: A Classification Problem. *ChemPhysChem* **2017**, *18*, 3266−3273.
(27) Wan, H.; Jiao, Y.; Bagger, A.; Rossmeisl, J. Three-Dimensional Carbon Electrocatalysts for CO2 or CO Reduction. *ACS Catal.* **2021**, *11*, 533−541.
(28) Wan, H.; Bagger, A.; Rossmeisl, J. Electrochemical Nitric Oxide Reduction on Metal Surfaces. *Angew. Chem., Int. Ed.* **2021**, *60*, 21966−21972.
(29) Bagger, A.; Wan, H.; Stephens, I. E. L.; Rossmeisl, J. Role of Catalyst in Controlling N2 Reduction Selectivity: A Unified View of Nitrogenase and Solid Electrodes. *ACS Catal.* **2021**, *11*, 6596−6601.
(30) Wan, H.; Østergaard, T. M.; Arnarson, L.; Rossmeisl, J. Climbing the 3D Volcano for the Oxygen Reduction Reaction Using Porphyrin Motifs. *ACS Sustainable Chem. Eng.* **2019**, *7*, 611−617.
(31) Gono, P.; Wiktor, J.; Ambrosio, F.; Pasquarello, A. Surface Polarons Reducing Overpotentials in the Oxygen Evolution Reaction. *ACS Catal.* **2018**, *8*, 5847−5851.
(32) Melander, M. M.; Kuisma, M. J.; Christensen, T. E. K.; Honkala, K. Grand-canonical approach to density functional theory of electrocatalytic systems: Thermodynamics of solid-liquid interfaces at constant ion and electrode potentials. *J. Chem. Phys.* **2019**, *150*, 041706.
(33) Rossmeisl, J.; Jensen, K. D.; Petersen, A. S.; Arnarson, L.; Bagger, A.; Escudero-Escribano, M. Realistic Cyclic Voltammograms from Ab Initio Simulations in Alkaline and Acidic Electrolytes. *J. Phys. Chem. C* **2020**, *124*, 20055−20065.
(34) Tayyebi, E.; Höskuldsson, A. B.; Wark, A.; Atrak, N.; Comer, B. M.; Medford, A. J.; Skúlason, E. Perspectives on the Competition between the Electrochemical Water and N_2 Oxidation on a TiO_2(110) Electrode. *J. Phys. Chem. Lett.* **2022**, *13*, 6123−6129.

https://doi.org/10.1021/acs.jpclett.2c02459
J. Phys. Chem. Lett. 2022, 13, 8928−8934